ORIGINAL RESEARCH ARTICLE

Lithium drop CuO nanocomposites synthesis and applications in adsorption

Nuha Abdul-Saheb Ridha¹, Noor Mustafa Kamal², Ahmed Neamah Thamer Al-Yasiri³, Shaymaa Hamzah Daylee⁴

- ^{1, 2} Department of Chemistry, University of Kufa, College of Science, Kufa, 540011, Iraq
- ³ Jabir Ibn Hayyan University for Medical and Pharmaceutical Sciences. Faculty of Pharmacy, Najaf Ashraf, 54001, Iraq
- ⁴ College of Education for Pure Sciences, University of Karbala, 56001, Iraq
- *Corresponding author: Noor Mustafa Kamal; Kamal; noorm.muhsin@uokufa.edu.iq

ABSTRACT

The co-precipitation method was used to synthesize lithium-doped copper oxide nanocomposites. Several techniques analyze these materials. X-ray diffraction was used to assess the crystal structure and nanoscale dimensions. Scanning electron microscopy (SEM) and energy dispersive spectroscopy (EDS) determined the elemental composition. The study also examined the effectiveness of the CuO-LiO nanocomposite in adsorbing blue crystalline dye from an aqueous solution. Adsorption was tested using UV-Vis spectroscopy with an equilibrium time of 30 min and a surface weight of 0.015 g. Results showed that the adsorption percentage ranged from 19.5% to 48% at temperatures between 298 and 323 K. The thermodynamic functions ΔH , ΔG , and ΔS were calculated to determine the effect of temperature, revealing an endothermic adsorption process.

Keywords: CuO nanoparticles; Lithium drop CuO nanocomposites; adsorption

ISSN: 2578-2010 (O)

ARTICLE INFO

Received: 4 September 2025 Accepted: 21 October 2025 Available online: 30 October 2025

COPYRIGHT

Copyright © 2025 by author(s). Applied Chemical Engineering is published by Arts and Science Press Pte. Ltd. This work is licensed under the Creative Commons Attribution-NonCommercial 4.0 International License (CC BY 4.0). https://creativecommons.org/licenses/by/4.0/

1. Background

Cupric oxide (CuO) is a recognized p-type semiconductor material (1) that has been active for gas sensors. CO oxidation reagents, solar energy conversion systems, and lithium-ion battery anode resources are distinguished by their low band-gap energy, robust catalytic activity, non-toxic properties, and cost efficiency. [1]. Like other metal oxides, CuO experiences inadequate electronic conductivity and significant volume fluctuations during the charge/discharge cycle, resulting in substantial mechanical stress and accelerated capacity degradation.^[2]. Numerous efforts have been undertaken to address the aforementioned issues, such as integrating carbon coatings, electronically conductive additives, or hierarchical nanostructures with varied morphologies. Recently, our team has shown considerable success in synthesizing CuO with diverse geometries through straightforward self-assembly.^[3] The catalytic characteristics of copper oxides can be substantially altered by adjusting particle porosity. [4]. their shape, their defect composition, or their size [5, 6]. Therefore, nanocrystalline copper(II) oxide is an ideal model for physical and chemical studies. Adsorption is the phenomenon of the accumulation of a substance in the form of molecules or ions on the surface of another substance. The substance to which adsorption occurs is called the adsorbate, and the surface on which adsorption occurs is called the adsorbent. Two types of adsorptions can be distinguished. The first is called physical adsorption, as physical adsorption involves natural forces of attraction between the adsorbing surface and the atoms, ions, or molecules adsorbed on the surface. Any special features do not characterize it [7]. The atom or molecule that undergoes physical adsorption is not chemically bound to the adsorbing surface. Instead, it occupies a specific surface area, which depends on the size of the adsorbed atoms or molecules. In general, the heat of physical adsorption is less than 40 kJ/mole and does not require activation energy. Physical adsorption is secondhand to control the surface area of solid resources according to well-known and approved methods in the study of surface chemistry. [8] The second category of adsorption is termed chemical adsorption, wherein surfaces create chemical interactions with the atoms, molecules, or ions adsorbed onto them. This form of adsorption is defined by its uniqueness, occurring under particular conditions on a designated surface, and may not manifest on an alternative surface under the same conditions.

The temperature of chemical adsorption may reach more than 80 KJ/mol, requiring activation energy. Its occurrence is localized on adsorption sites characterized by the lowest potential energy. [9].

2. Materials

CuCl₂.2H₂O, LiCl, Fig leaf extract, sodium hydroxide, and ethanol.

2.1. Preparation of Fig leaf extract

Wash six grams of fig leaves with deionized water and dry them. Combine five grams of leaves with 400 milliliters of D. water. Heat and stir at 80°C for 45 minutes. Filter the extract and collect the filtrate in a clean beaker [10], Then pulverized, as seen in **Figure 1**.

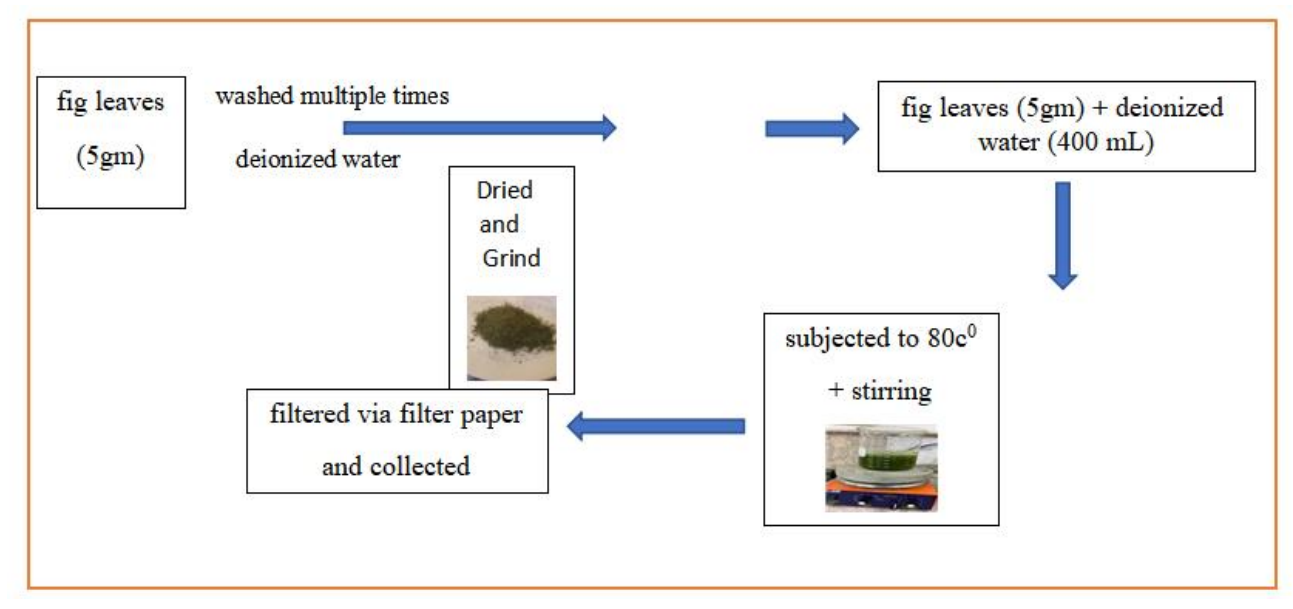


Figure 1. Preparation of Fig leaf extract

2.2. Preparation of CuO nanoparticles

2. 0.675 g of CuCl₂·2H₂O was measured and sited in a beaker, and 1000 ML of D. water was added with continuous stirring until complete dissolution occurred. Using a burette, 25 ML of fig leaf extract was incrementally dispensed in drops with continuous agitation at 20°C. Then, the temperature was higher to 80°C, and a 1 M sodium hydroxide solution was additional under vigorous stirring until the pH reached 10 and a dark brown precipitate emerged. The precipitate was obtained using filtration and subsequently centrifuged after the mixture was allowable to cool to ambient temperature. The quartz was washed away

with D.water and ethanol to remove impurities, shadowed by drying in an oven at 80°C for two h. to eliminate hydroxide.

2.3. Preparation of lithium drop CuO composites

Preparation of Lithium-doped CuO nanocomposites by using two method:

The First method (CL1): 0.1 g of CuO nanoparticles was incorporated into 100 ML of fig leaf extract at 80 °C for thorough immersion, a mole ratio of 1:1, 0.05 g of LiCl was incorporated into the postponement, and the amalgamation was subjected to magnetic stirring for 10 min . Subsequently, 0.05 M NaOH was added to the mixture, resulting in a ending pH of 9, and was magnetically agitated aimed at 30 min at 80 °C. Ultimately, CuO adorned with lithium nanoparticles was subjected to several washes with D.water, shadowed by filtering and air drying at 90°C for seven h., and then calcined at 400°C for two h.

The second method (CL2): The conventional new protocol for the nanocomposite with a mole ratio of 1:1 is defined below: 1 g of CuCl₂·2H₂O was dissolved in fig leaf extract at 80 °C, and the mixture was magnetically stirred for 10 min . Next, 0.2488 g of LiCl was added to the suspension. Then, 0.2 M NaOH was added to the previously described mixture, achieving a ending pH of 9, and the solution was magnetically stirred used for 30 minutes at 80 °C. Ultimately, CuO adorned with lithium nanoparticles was subjected to several washes with D. water, filtered, air dried at 90°C for seven h., and subsequently calcined at 400°C for two h.

3. Results and discussion

3.1. X-Ray

As shown in **Figure 2**, the XRD patterns of CuO nanowires are consistent with the standard card, aligning well with JCPDS card number 45-0937 (CuO). The absence of other diffraction peaks indicates the purity of the CuO nanowires. The characteristic peaks at 35.5° and 38.7° are the crystal planes of the monumental CuO phase, which indicates the decent crystallinity of CuO [11]. Average crystal diameter (D) is calculated using Equation (1)^[13-12].

$$D = \lambda / \beta \cos(\theta) \dots (1)$$

In this context, where K = 0.9 is the shape factor, λ denotes the wavelength of the X-rays, β signifies the full width at half maximum (FWHM), and θ indicates the Bragg angle. The computed average crystallite size of the CuO nanoparticles is 29.26 nm.

Analysis of Figure (3a) confirmed the appearance of new peaks and shifts in the values of CuO, 31.3, 47.8, 52.2, 57.1, 65.0, and 66.6. As for Figure (3 b), the same peaks appeared, but with slight shifts and also a difference in the intensity of the peaks, indicating the effect of the preparation method using salts or using nanomaterials, as well as the occurrence of shifts in some peaks, which suggests the presence of CuO and Li within the compound. The relative intensity of diffraction peaks suggests that the CuO content is much higher than the Li content, as evidenced by the distinct and sharp diffraction peaks.

The calculated crystallite size of CuO/Li(CL1) and CuO/Li(CL2) nanoparticles is between 19-6 nm and 17-6 nm, and the average is 9.4 nm and 8.6 nm, respectively.

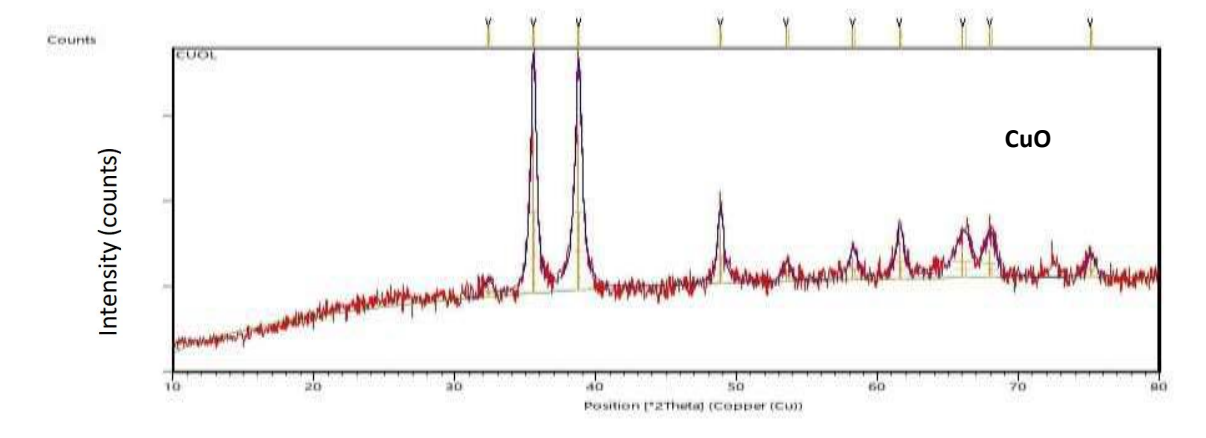
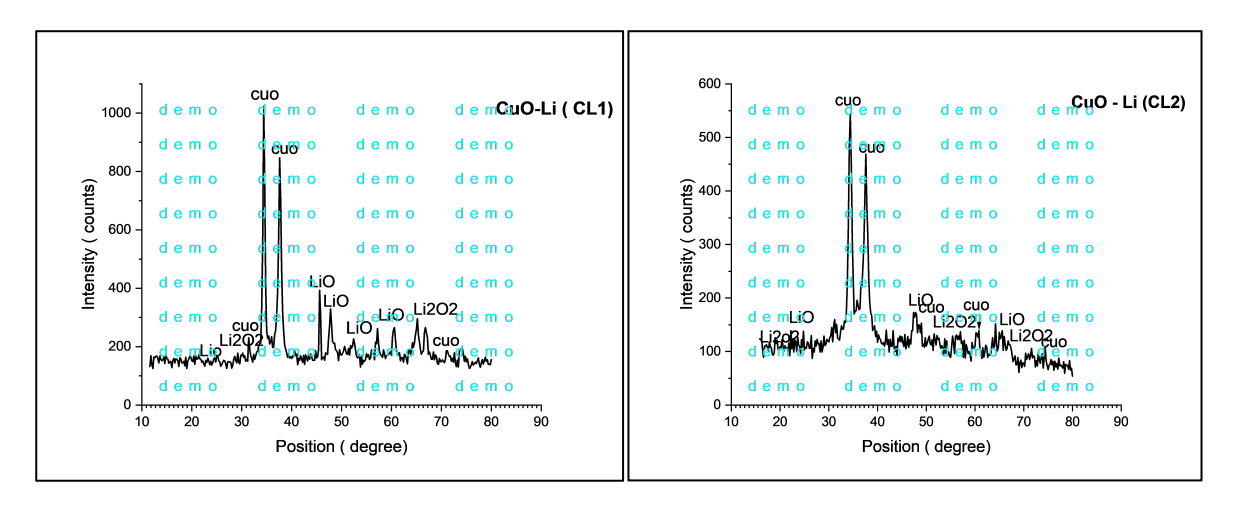


Figure 2. XRD pattern of CuO nanoparticle



Figures 3. Patterns of CuO / Li nanocomposite by using different methods.

3.2. **SEM**

Figure 4 of the scanning electron microscope images shows regular spherical shapes ^[12]. The size of the nanoparticle was calculated to be 29.3 nm. Structural modification, The morphology and dimensions of the nanostructures in the (CuO/Li) nanocomposite differ from those of the original copper oxide nanoparticles, indicating that lithium doping has effectively transformed the structure. The average dimensions of the resultant nanocomposite are said to be roughly (63.71) nm and (70.92) nm, as depicted in Figures (5) and (6), Impact of the method. The study methodology influences the ultimate form and dimensions of the nanocomposite, a common finding in nanoparticle production. The transition from pure (CuO) to the (CuO/Li) nanocomposite is directly attributable to the employed synthesis process^[13].

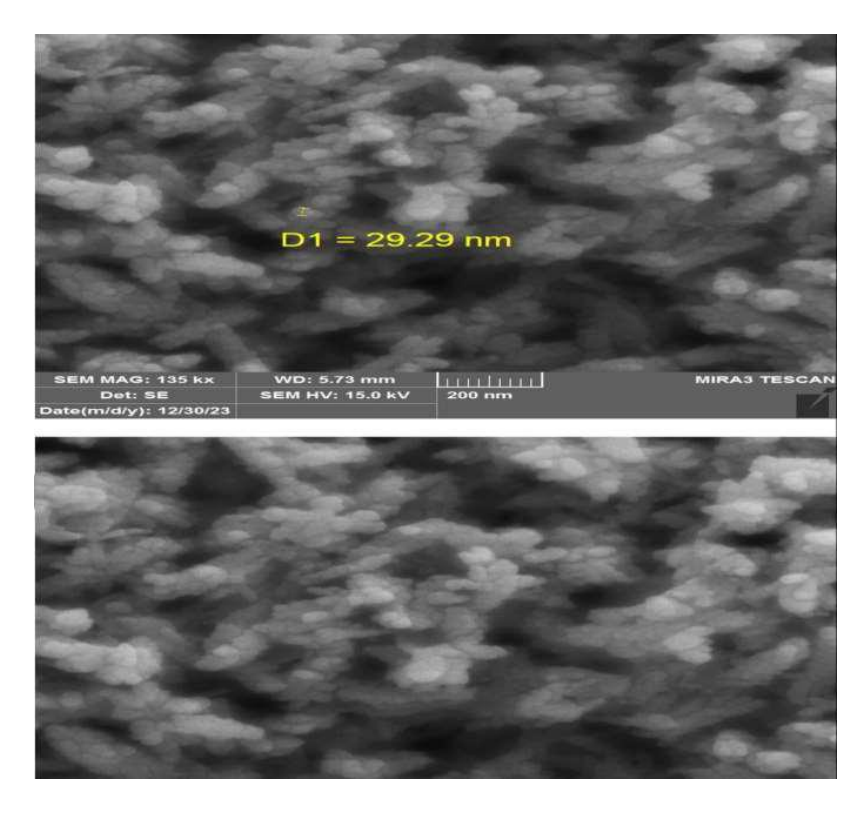


Figure 4. FESEM images of CuO nanoparticles

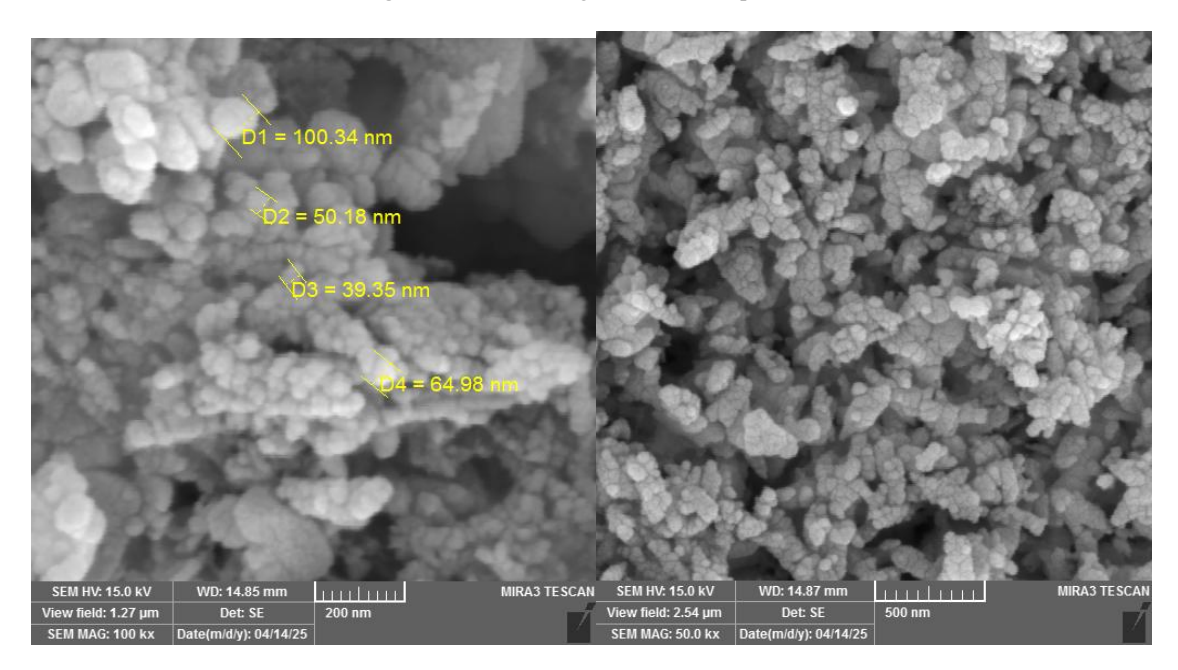


Figure 5. FESEM images of CuO/Li (CL1) nanocomposites by the First method

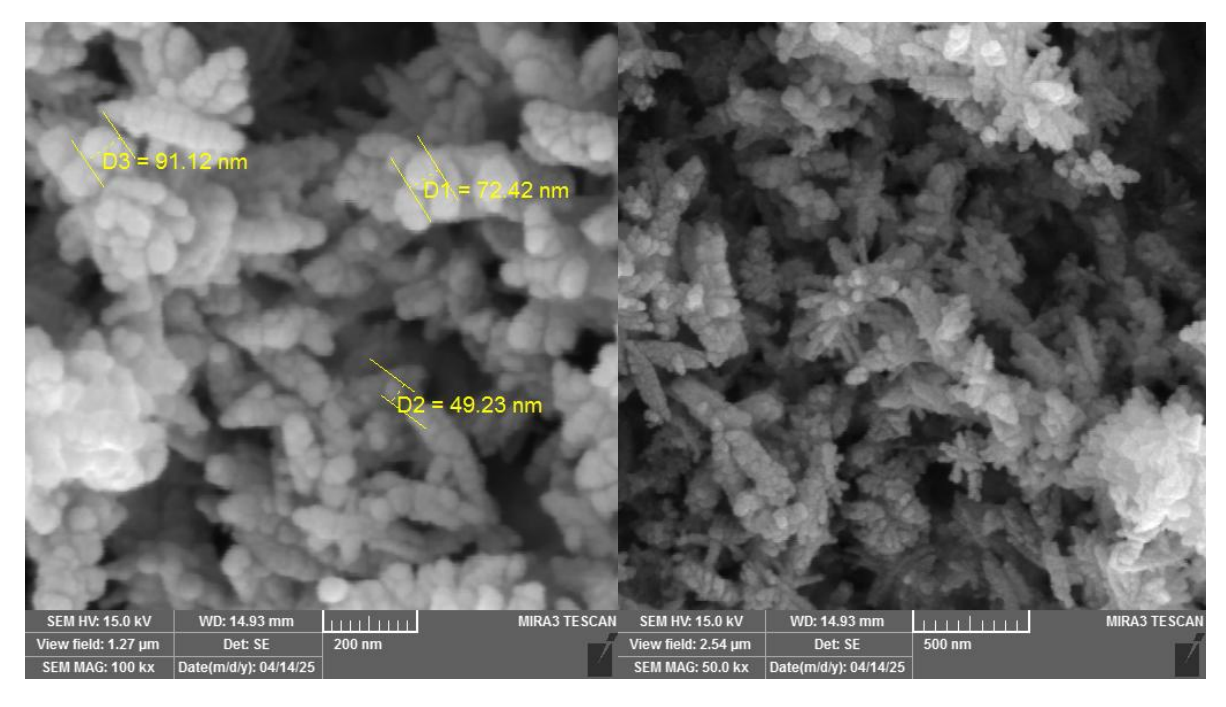


Figure 6. FESEM images of Cuo/Li (CL2) nanocomposites by the second method

3.3. EDS

The results presented in **Figure 7**, The EDX analysis indicates that the CuO nanoparticles exhibit high purity, with a copper content of 76.15% and an oxygen content of 13.75%, along with minimal impurities. ^[14] Some studies indicate that when sodium hydroxide is used as the solvent, the EDX spectrum shows closer alignment with the stoichiometric ratio compared to when ammonium hydroxide is used ^[15]. The concentration of Cu was elevated, indicating that the synthesized CuO nanoparticles were nearly stoichiometric. The results presented in Figure 8 reveal a disparity in the elemental weight ratios of the nanocomposites compared to the CuO nanoparticles, highlighting the influence of the synthesis procedure on the elemental ratios, morphology, and mass of the nanocomposites, as shown in **Table 1**.

Table 1. The presence of element

nanocomposites	Element	W%
CuO nanoparticles		
	Cu	76.15
	O	13.75
CuO/Li(CL1)	Cu	65.02
	O	19.20
	Li	15.10
CuO/Li(CL2)	Cu	62.75
	O	25.05
	Li	12.04

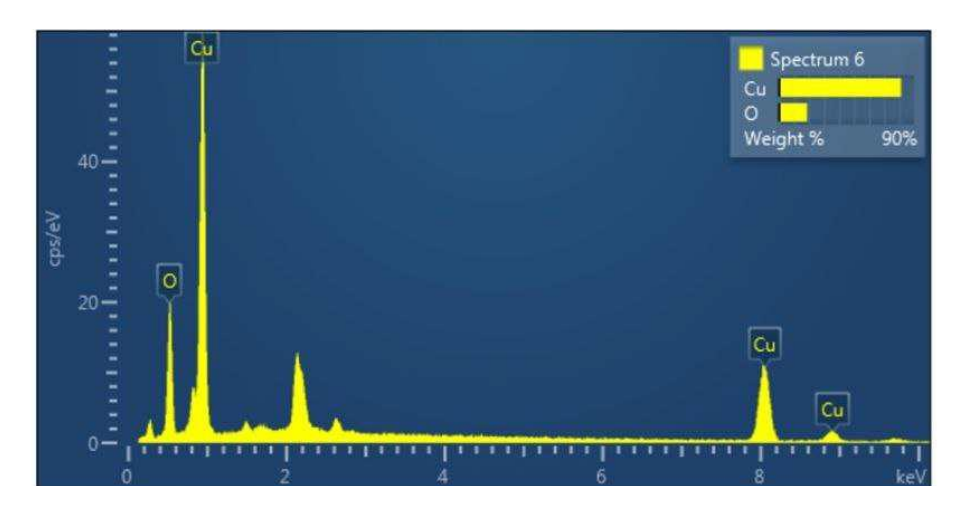


Figure 7. EDX of CuO nanoparticle

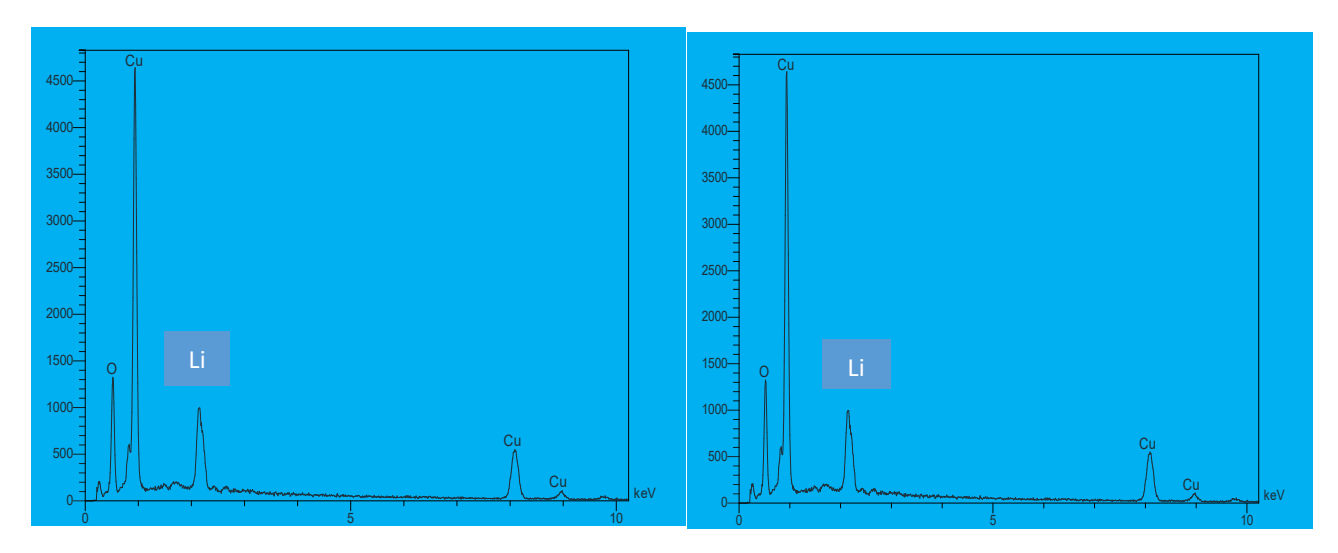


Figure 8. EDX of CuO / Li nanocomposites

3.4. Adsorption

The capacity of the nanocomposite to adsorb the blue crystalline dye from its aqueous solutions was examined, following the measurement of the dye's maximum wavelength, which was resolute to be 628nm, as illustrated in **Figure 9**.

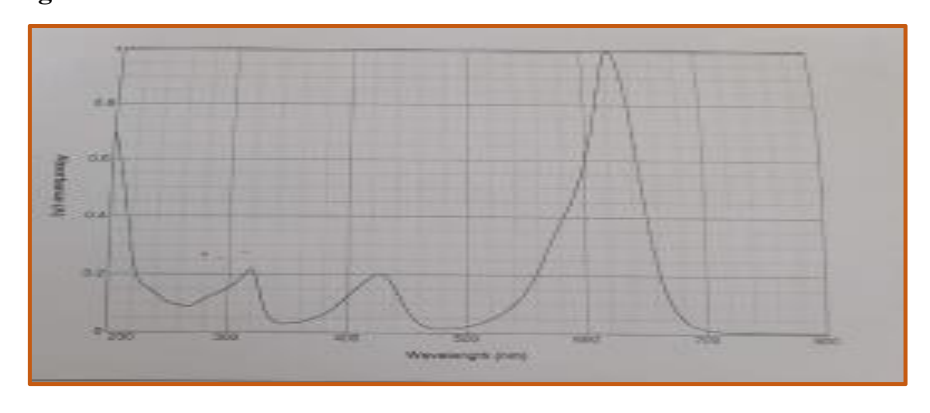


Figure 9. Dye's maximum wavelength

3.5. Preparation of the adsorbent crystalline blue (C.B.C)

500 ML of dye was formulated at 100 ppm via dissolving 0.05 g in 500 mL of distilled water. The remaining solutions were generated at concentrations of 1, 3, 5, 7, and 9 ppm through dilution.

3.6. Calibration curve for crystal blue brilliant (C.B.C)

The absorbance values of five concentrations of the produced dye (1-9 ppm) were measured using a UV-Visible spectrophotometer to construct a standard calibration curve, as shown in **Figure 10**.

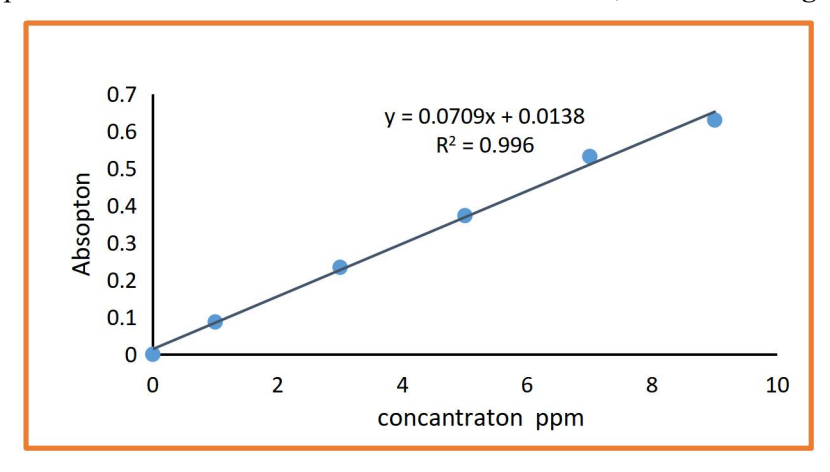


Figure 10. Calibration curve of dye's

3.7. Adsorption isotherm

Figure 12 illustrates the adsorption isotherm ^[16] of the crystalline blue dye at 298 K by the nanocomposite. The proportion of adsorbed material rose with higher dye concentrations. The percentage is dictated by legislation:

Percentage of Removal % =
$$\frac{A0}{A0-A}$$
 * 100%

A₀: The quantity of dye absorption prior to the adsorption procedure.

A: The quantity of dye absorption following the adsorption procedure.

The adsorption isotherm was determined to conform to the (S5) model as per the Gilles classification, as illustrated in **Figure 11**.

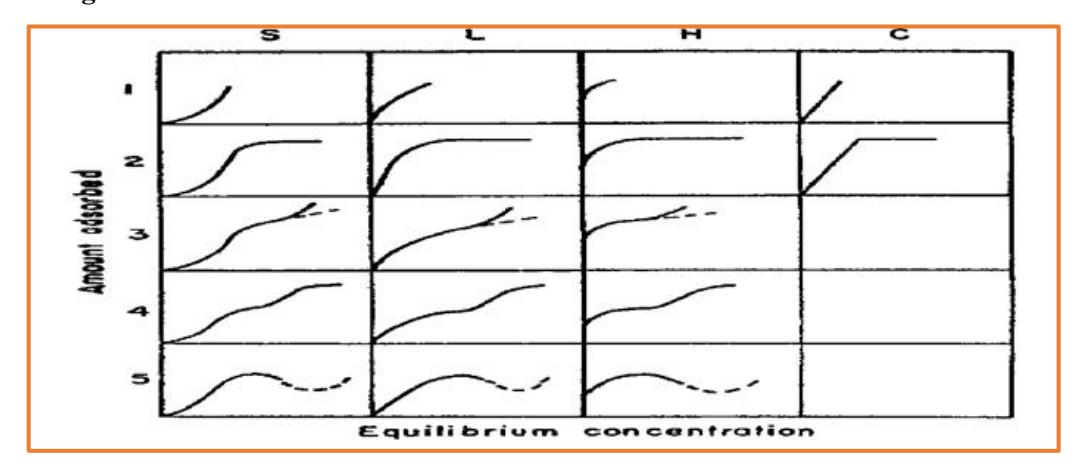


Figure 11. the Gilles classification to adsorption isotherms

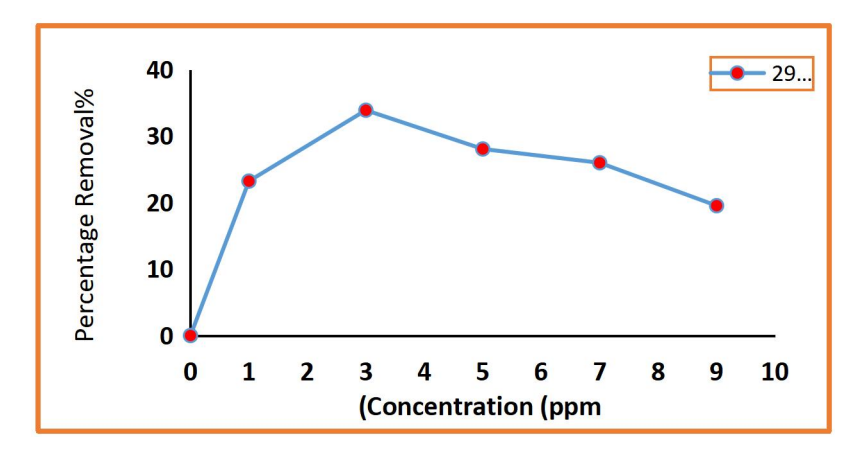


Figure 12. the adsorption isotherm of dye at 298 K

3.8. Langmuir model

The Langmuir model posits that a finite figure of active sites exists on the surface, directly proportionate to the adsorbent's surface area. Each site is limited to the adsorption of a single molecule, which is attached by either chemical or physical connections. Consequently, adsorption transpires on the surface in a monolayer configuration.

The linear equation representing the Langmuir model can be articulated numerically as follows^[17]:

Qe =
$$\frac{Ce}{Qe} = \frac{1}{a} + \frac{b}{a}$$
. Ce

The graphical relationship between (Ce) and (Ce/Qe) allows for the estimation of constant values via the slope of the linear graph and the intersection point, as illustrated in **Figure 13**, using **Table 2** utilized for plotting.

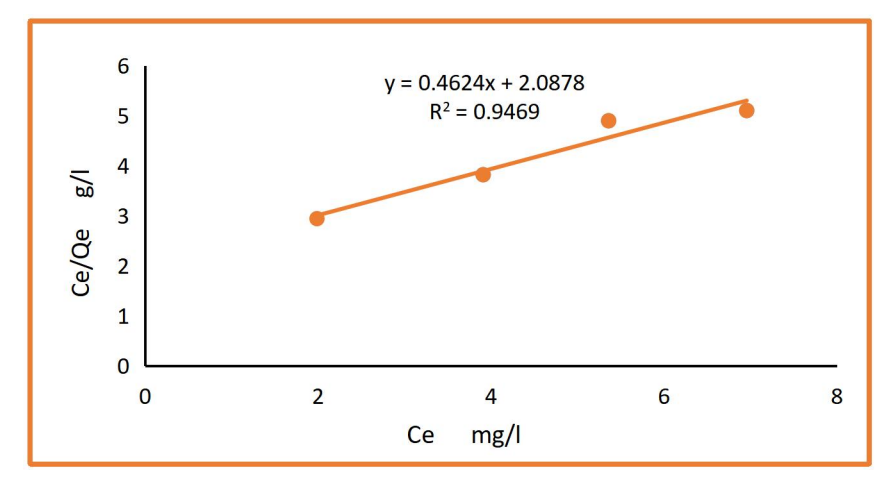


Figure 13. Langmuir equation in linear form for dye adsorption at 298K and PH=7

Table 2. Value of C_e , C_e/Q_e , $Log C_e$ and $Log Q_e$ for dye at 298K and PH=7

C ₀ mg/L	Ce mg/L	$rac{\mathrm{C_{e}/Q_{e}}}{\mathrm{g/L}}$	Log C _e mg/L	Log Q _e mg/g
1	0.977	2.9437	0.2981	-0.1706
3	3.9.9	3.8225	0.5552	-0.0271
7	5.359	4.9008	0.7291	0.0386
9	6.956	5.1054	0.8423	0.13433

3.9. Freundlich model

This model characterizes an adsorption system, illustrating the variation in the quantity of adsorbed material per unit area or mass of the adsorbent relative to the equilibrium concentration [18]. The linear relationship for this model is stated as ($Log \ Qe=Log \ Kf+1/n \ LogCe$), as illustrated in **Figure 14**, with **Table 2** utilized for plotting.

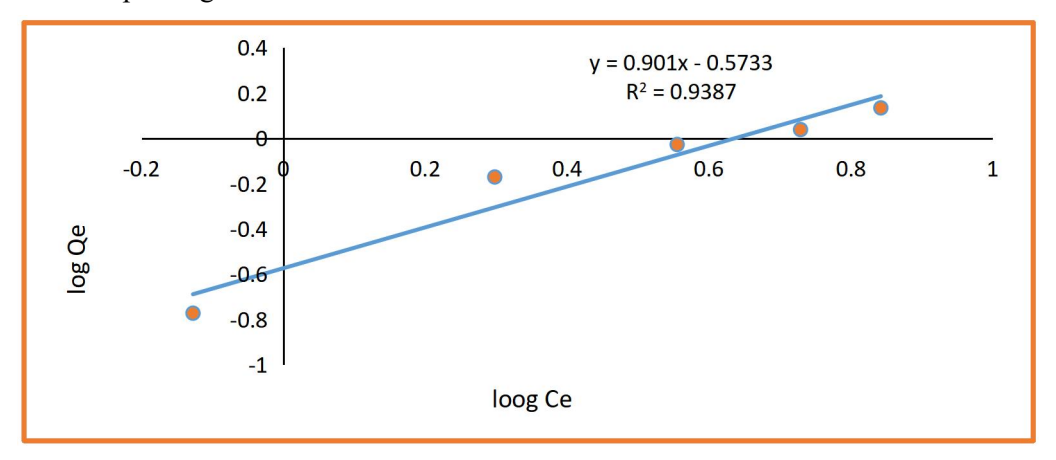


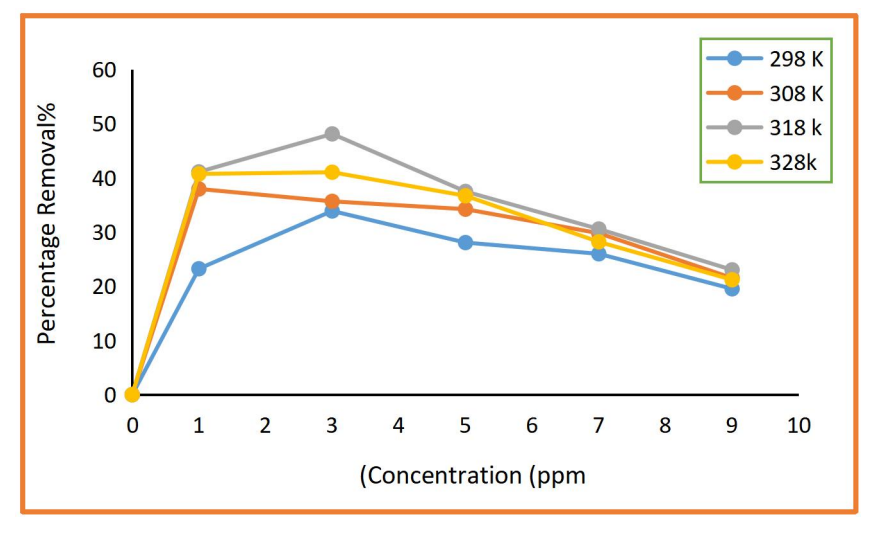
Figure 14. Linear form of Freundlich equation for the adsorption of dye at 298K

3.10. The effect of temperature on the adsorption rate

A study was shown on the result of temperature on the dye Percentage Removal at different temperatures within the range (298-328 k) and (pH= 7), as illustrated in **Figure 15**, with **Table 3** utilized for plotting.

Percentage Removal % Concentration (ppm) 298 k 308 k318 k 328 k 1 23.214 37.93 41.071 40.7 3 33.87 35.64 48.08 41.01 5 28.04 34.2 37.466 36.666 7 25.97 29.77 30.543 28.176 9 19.52 21.513 23.01 21.184

Table 3. Percentage Removal for dye at different temperatures



3.11. Calculating the thermodynamic values for the adsorption process

1.7 1.68 1.66

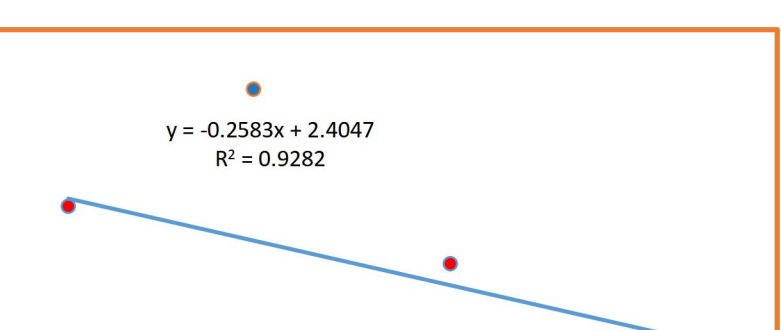
1.64

1.62 1.6 1.58 1.56 1.54 1.52

3.05

3.1

The value of ΔH was determined by graphing the logarithm of Xm versus the reciprocal of temperature, as illustrated in **Figure 16**,in accordance with the van't-Hoff equation^[19]:



3.2

1/T *10-3

3.25

3.3

3.35

3.4

 $Log~Xm = -\Delta H ~/~ 2.303~RT + ~Const.$

Figure 16. The altered Vant Hoff's equation for dye adsorption at various temperatures

3.15

From the aforementioned linear relationship, the value of ΔH is resulting from the slope (slope = $\Delta H/2.303R$). The value of ΔG can be computed to ascertain whether the adsorption process is spontaneous or non-spontaneous under these conditions, as per the equation ($\Delta G = RT \ln(Qe/Ce)$). Utilizing Gibbs' equation ($\Delta G = \Delta H - T\Delta S$), the entropy value ΔS is obtained, which reflects the arrangement of the adsorbed molecules on the surface.

 Table 4. The thermodynamical parameters values

 Dye
 Constant
 ΔG KJ.mol⁻¹
 ΔH J.mol⁻¹
 ΔS J.mol⁻¹.K⁻¹

 C.B.C
 2.4047
 -36.7615
 49.457
 -28.932

The data presented in **Table 4** The positive enthalpy values confirm the endothermic nature of the adsorption process, whereas the negative free energy values indicate that the process occurs spontaneously under the specified conditions. Furthermore, the negative entropy values suggest that the adsorbed molecules are more orderly on the adsorbent surface than in the liquid phase, as they occupy specific sites and follow defined pathways, forming a distinct structural arrangement.

4. Conclusion

Copper oxide monooxygenase nanoparticles (CuO NPs) were synthesized, and the results of various characterization analyses showed good agreement with previously reported data. The precursor material, CuCl₂·2H₂O, was reacted with sodium hydroxide (NaOH) at a concentration of 1 M. A nanocomposite with an average diameter of 1 nm and a uniform spherical morphology was successfully obtained. The composite was subsequently doped with lithium using two approaches: the first involved employing a nanomaterial containing a lithium salt, while the second combined copper and lithium salts. In both methods, sodium hydroxide was used at a concentration of 0.05 M. The results demonstrated a clear influence of the synthesis method on the size, morphology, and compositional ratios of the resulting composites. This study enhances the understanding of doped nanoparticle synthesis with controlled morphologies and desirable properties for potential applications in various fields. Expressions of Gratitude

The writers express their sincere gratitude to the staff of the Graduate Studies Laboratory in the Department of Chemistry, College of Science, University of Kufa, for providing access to laboratory facilities and support during this research.

Conflict of interest

The authors declare no conflict of interest.

References

- 1. Xiang, J., et al., Enhanced high rate properties of ordered porous Cu2O film as anode for lithium ion batteries. Electrochimica Acta, 2010. 55(17): p. 4921-4925.
- 2. Mishra, S.R. and M. Ahmaruzzaman, CuO and CuO-based nanocomposites: Synthesis and applications in environment and energy. Sustainable Materials and Technologies, 2022. 33: p. e00463.
- 3. Mai, Y., et al., CuO/graphene composite as anode materials for lithium-ion batteries. Electrochimica Acta, 2011. 56(5): p. 2306-2311.
- 4. Zhou, M., et al., Carbonate-assisted hydrothermal synthesis of nanoporous CuO microstructures and their application in catalysis. 2010, Wiley Online Library.
- 5. Sadykov, V., et al., Catalytic oxidation of CO on CuOx revisited: Impact of the surface state on the apparent kinetic parameters. Catalysis Today, 2009. 144(3-4): p. 324-333.
- 6. Svintsitskiy, D.A., et al., In situ XRD, XPS, TEM, and TPR study of highly active in CO oxidation CuO nanopowders. The Journal of Physical Chemistry C, 2013. 117(28): p. 14588-14599.
- 7. Kalam, S., et al., Surfactant adsorption isotherms: A review. ACS omega, 2021. 6(48): p. 32342-32348.
- 8. Liu, R.S., et al., Advances in post-combustion CO2 capture by physical adsorption: from materials innovation to separation practice. ChemSusChem, 2021. 14(6): p. 1428-1471.
- 9. Sameer, M., K. Hussein, and A. Saadon, Isa, The ability of attapulgite clay as a physical antidote in adsorption of some drugs from solution. Iraqi J. Sci. A, 2001. 42: p. 80-98.
- 10. Gottimukkala, K., R. Harika, and D. Zamare, Green synthesis of iron nanoparticles using green tea leaves extract. J. Nanomed. Biother. Discov, 2017. 7(1): p. 151.
- 11. Ashok, C., K.V. Rao, and C.S. Chakra, Structural analysis of CuO nanomaterials prepared by novel microwave-assisted method. Journal of Atoms and Molecules, 2014. 4(5): p. 803-806.
- 12. Ahamed, M., et al., Synthesis, characterization, and antimicrobial activity of copper oxide nanoparticles. Journal of Nanomaterials, 2014. 2014(1): p. 637858.
- 13. Cazan, C., A. Enesca, and L. Andronic, Synergic effect of TiO2 filler on the mechanical properties of polymer nanocomposites. Polymers, 2021. 13(12): p. 2017.
- 14. Sriram, G., et al., Mg–Al-layered double hydroxide (LDH) modified diatoms for highly efficient removal of Congo red from aqueous solution. Applied Sciences, 2020. 10(7): p. 2285.
- 15. Patel, M., et al., Synthesis of ZnO and CuO nanoparticles via Sol gel method and their characterization by using various techniques. Discover Materials, 2022. 2(1): p. 1.
- 16. Musah, M., et al., Adsorption kinetics and isotherm models: a review. CaJoST, 2022. 4(1): p. 20-26.
- 17. Islam, M.A., et al., Langmuir adsorption kinetics in liquid media: interface reaction model. ACS omega, 2021. 6(22): p. 14481-14492.
- 18. Pereira, S.K., et al., A simplified modeling procedure for adsorption at varying pH conditions using the modified Langmuir–Freundlich isotherm. Applied Water Science, 2023. 13(1): p. 29.
- 19. Carrero, J., Application of the van't Hoff Equation to Phase Equilibria. ChemTexts, 2024. 10(3): p. 4.